Geochronology and geochemistry of subducted Cadomian continental basement in central Iran: Decompressional anatexis along the Jurassic Neotethys margin

Article *in* Gondwana Research · February 2020

DOI: 10.1016/j.gr.2020.01.005

Rezvaneh Jamali Ashtiani
Shahid Beheshti University

Jamshid Hassanzadeh
California Institute of Technology

Masafumi Sudo
Universität Potsdam

Christina Günter
Universität Potsdam

Gondwana Research xxx (xxxx) 1–11

Contents lists available at ScienceDirect

Gondwana Research

journal homepage: http://ees.elsevier.com

Geochronology and geochemistry of subducted Cadomian continental basement in central Iran: Decompressional anatexis along the Jurassic Neotethys margin

Rezvaneh Jamali Ashtiani [a,*], Jamshid Hassanzadeh [b], Axel K. Schmitt [c], Masafumi Sudo [d], Martin Timmerman [d], Christina Günter [d], Edward Sobel [d]

[a] Faculty of Earth Sciences, Shahid Beheshti University, Tehran, Iran
[b] Division of Geological and Planetary Sciences, California Institute of Technology, Pasadena, CA 91125, USA
[c] Universität Heidelberg, Institut für Geowissenschaften, 69120 Heidelberg, Germany
[d] Universität Potsdam, Institut für Geowissenschaften, 14476 Potsdam-Golm, Germany

ARTICLE INFO

Article history:
Received 9 October 2019
Received in revised form 4 December 2019
Accepted 6 January 2020
Available online xxx
Handling Editor: T. Gerya

Keywords
Neotethys Ocean
Jurassic subduction
High-pressure metamorphism
Eclogite
Partial melting

ABSTRACT

Late Neoproterozoic-Early Cambrian calc-alkaline granitoids are ubiquitous in the continental basement of Iran and indicate formation within a Cadomian arc system at the northern margin of Gondwana. A basement complex comprising mainly mica schist, paragneisses, and metagranite along with metabasite and rare pegmatite is exposed in the Zayanderud region north of Shahrekord located in the hinterland of the Zagros mountain range. This complex is unique in the Neotethyan realm because it includes eclogites with Jurassic metamorphic ages implying involvement of continental crust at the onset of subduction. Ion microprobe U—Pb zircon dating along with trace element and oxygen isotope analyses for metagranites define two zircon age clusters of ca. 552 and 565 Ma confirming connection with the other Ediacaran age basement arc plutons in the belt. Zircon geochronology for pegmatite, by contrast, yielded a concordant age population averaging 176.5 ± 3.3 (2σ) Ma. Zircon crystals from the pegmatite also have unusually low rare earth element (REE) abundances with sharp increases towards the heavy REE. Along with an absence of a negative Eu anomaly, this indicates a high-grade metamorphic origin of zircon crystallizing from a pegmatite which was formed by melting of mica schist and possibly amphibole eclogite during decompression where incipient garnet breakdown released Zr and HREE to form zircon, and LREE were retained in stable apatite and titanite. Corresponding $^{40}Ar/^{39}Ar$ phengite dates from the pegmatite and the mica schist country-rock are overlapping with or only slightly postdate the U—Pb zircon ages, indicating rapid cooling after reaching maximum metamorphic pressure in the Early Jurassic. The Zayanderud basement complex is thus potentially a rare example of deep burial of continental crust and rapid exhumation due to buoyant escape during the incipient stages of subduction, well before the ultimate closing of the Neotethys ocean basin between Arabia and Eurasia in the mid-Tertiary.

1. Introduction

The increasing availability of U—Pb zircon age data for Iran and the neighboring terranes now reveals that the late Neoproterozoic was an episode of immense continental growth in the region by addition of magma from the mantle during the final stages of Gondwana supercontinent assembly (Condie, 2014). This major crust formation event is linked to extensive and complex magmatic arc development which led to intrusion of Ediacaran-Early Cambrian (ca. 635 Ma to 520 Ma) calc-alkaline granitoids all along the northern periphery of Gondwana (Stern, 1994). Recent U—Pb zircon geochronology and compositional data for granitoids from most structural zones of the Iranian basement have confirmed their origin in Cadomian arc systems which are also observed in various terranes from southern Europe to Turkey and farther east (Stern, 1994; Hassanzadeh et al., 2008; Moghadam et al., 2016). Late Paleozoic rifting and continental rupture progressing to a passive continental margin was followed by closure of the resulting Neotethys ocean during mid-Tertiary times (Hassanzadeh and Wernicke, 2016 and references therein; Pirouz et al., 2017). The subsequent collision between Arabian and Eurasian continental plates exposed high-grade metamorphic rocks in the Zayanderud metamorphic complex (ZMC) located in the hinterland of the Zagros mountain chain, which are unique in providing excellent opportunities for studying the transition from a passive margin to an Andean-type subduction zone. Two major uncertainties related to the ZMC are the ages of protolith formation and the timing of peak metamorphism. Protolith ages have been presumed to be Precambrian based on inferred cross-cutting by late Neoproterozoic metagranites (Malek-Mahmoudi et al., 2017). Therefore, determination of the magmatic age of the metagranites is key for constraining the unknown timing of protolith formation. The existing age data of these metagranites is highly variable from Ediacaran (Nutman et al., 2014; Davoudian et al., 2016) to Middle Jurassic (Hosseini and Ahmadi, 2016), indicating multiphase plutonism in the region. More recently, however, the veracity of Jurassic dates has been challenged by attributing middle Cambrian magmatic ages to the metagranites (Badr et al., 2018). $^{40}Ar/^{39}Ar$ phengite dates from different lithologies in the ZMC mostly indicate Middle Jurassic cooling, but there is ambiguity regarding the timing of deep burial of ZMC eclogites and their subsequent thermal his-

* Corresponding author.
E-mail address: rja.rezvaneh@gmail.com (R. Jamali Ashtiani)

tory. To resolve these unsettled ambiguities regarding the Jurassic evolution of the ZMC, we present $^{40}Ar/^{39}Ar$ phengite dates for a newly discovered anatectic pegmatite and its host mica schist along with U—Pb ages, trace element, and oxygen isotopic compositions for zircon from the anatectic pegmatite. Jurassic zircon ages for the anatectic pegmatite indicate that peak metamorphism postdates eclogite formation, which suggests that a passive continental margin assemblage of metasediments and local metabasites in the ZMC experienced rapid burial, metamorphism, and exhumation during subduction initiation of the Neotethys Ocean.

2. Tectonic setting

The NW-trending Sanandaj-Sirjan Zone (SSZ) is situated to the northeast of the Main Zagros Thrust (MZT) in Iran (Fig. 1). The pre-Permian substrate of the SSZ is analogous to Arabia-Nubia (Berberian and King, 1981) and includes calc-alkaline granitoid plutons with crystallization ages of ca. 600–500 Ma (e.g., Ramezani and Tucker, 2003). Those plutons developed along a continental arc along the northern Gondwana active margin during the late Neoproterozoic Cadomian orogeny (Hassanzadeh et al., 2008; Moghadam et al., 2016). The metamorphic-plutonic basement blocks of the SSZ are exposed in fault-bounded blocks placed against younger unmetamorphosed strata along faults extending for 10s of km.

After the formation of the Neotethys Ocean in late Paleozoic times, the SSZ segment of central Iran began developing as an Atlantic-type rifted margin throughout the Permian and Triassic times based on the carbonate ramp deposits preserved in both sides of the MZT. Arc magmatism commenced along the Eurasian continental margin above a NE-dipping subduction zone in Late Triassic-Early Jurassic time (Hassanzadeh and Wernicke, 2016 and references therein). The Mesozoic arc is manifested by a well-developed chain of calc-alkaline plutonic and volcanic centers (Hassanzadeh and Wernicke, 2016). In the case of the Zayanderud region presented in this contribution, Jurassic arc volcanics have been mapped (Zahedi, 1976, 1993) and dated (Emami and Khalili, 2014), but the existence of age-equivalent granitoids has been controversial (Ghasemi et al., 1996; Hosseini and Ahmadi, 2016; Badr et al., 2018).

3. Geology of the studied area

The studied basement block crops out along the Upper Zayanderud River, ~50 km north of the MZT (Figs. 1 and 2). Outcrops occur around the Zayanderud dam lake, near the town of Chadegan, and extend downstream from the dam for several tens of km (Figs. 1 and 2). Covering an area of ~800 km^2, the ZMC consists of preferentially erodible schistose rocks and is largely concealed underneath Neogene lacustrine sediments. Consequently, the ZMC rocks are best exposed along the walls of the deeply incised Zayanderud canyon be-

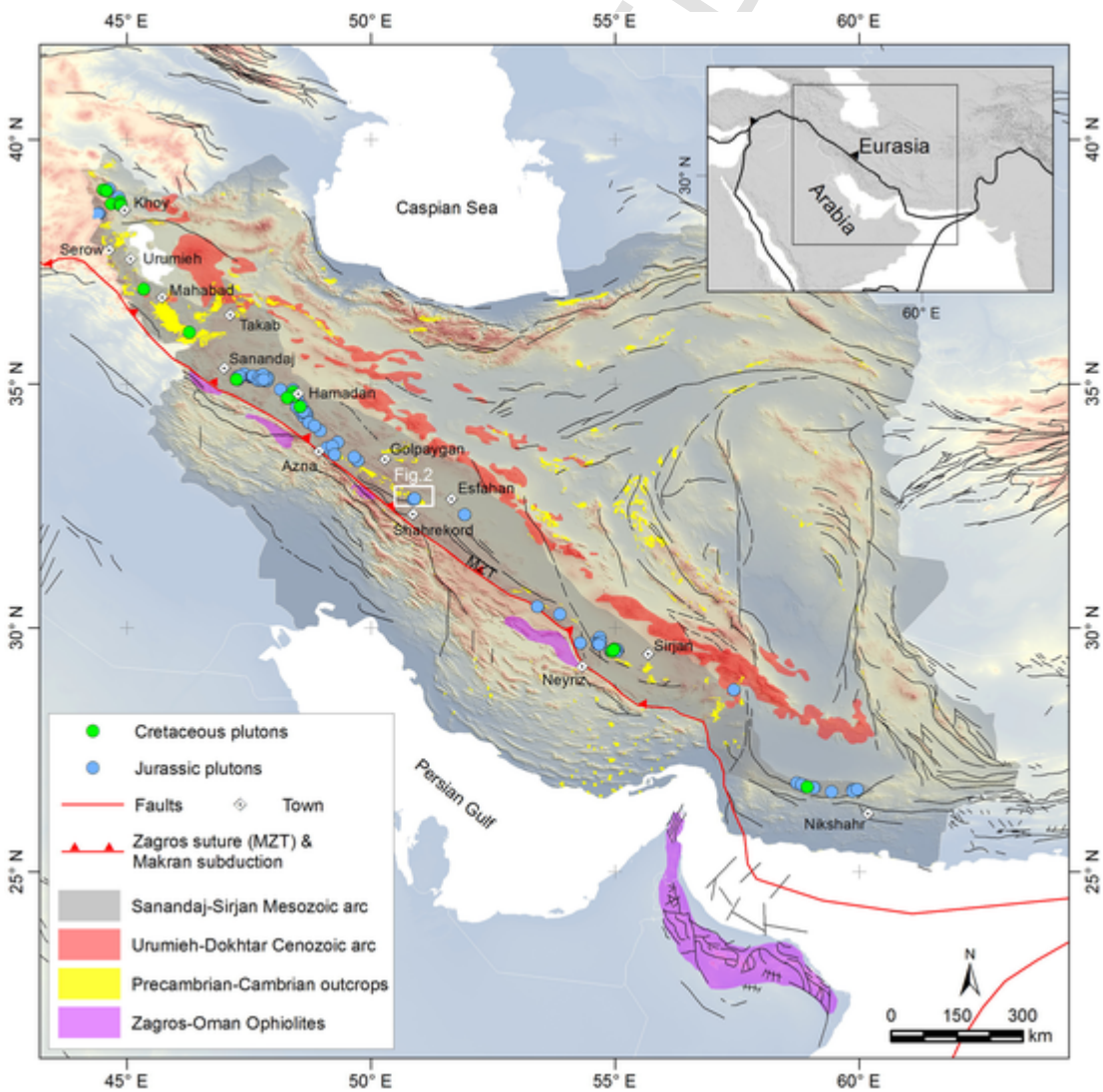

Fig. 1. Simplified geologic map of Iran over digital elevation model shaded relief map (after Geological Survey of Iran maps), showing the studied area in Sanandaj-Sirjan zone (SSZ) on the NE side of the Main Zagros Thrust (MZT). Mesozoic calc-alkaline arc plutons are shown to emphasize localized high heat flow during the Jurassic and Cretaceous times (Hunziker et al., 2015; Hassanzadeh and Wernicke, 2016 and references therein; Lechmann et al., 2018; Yang et al., 2018; Azizi and Stern., 2019).

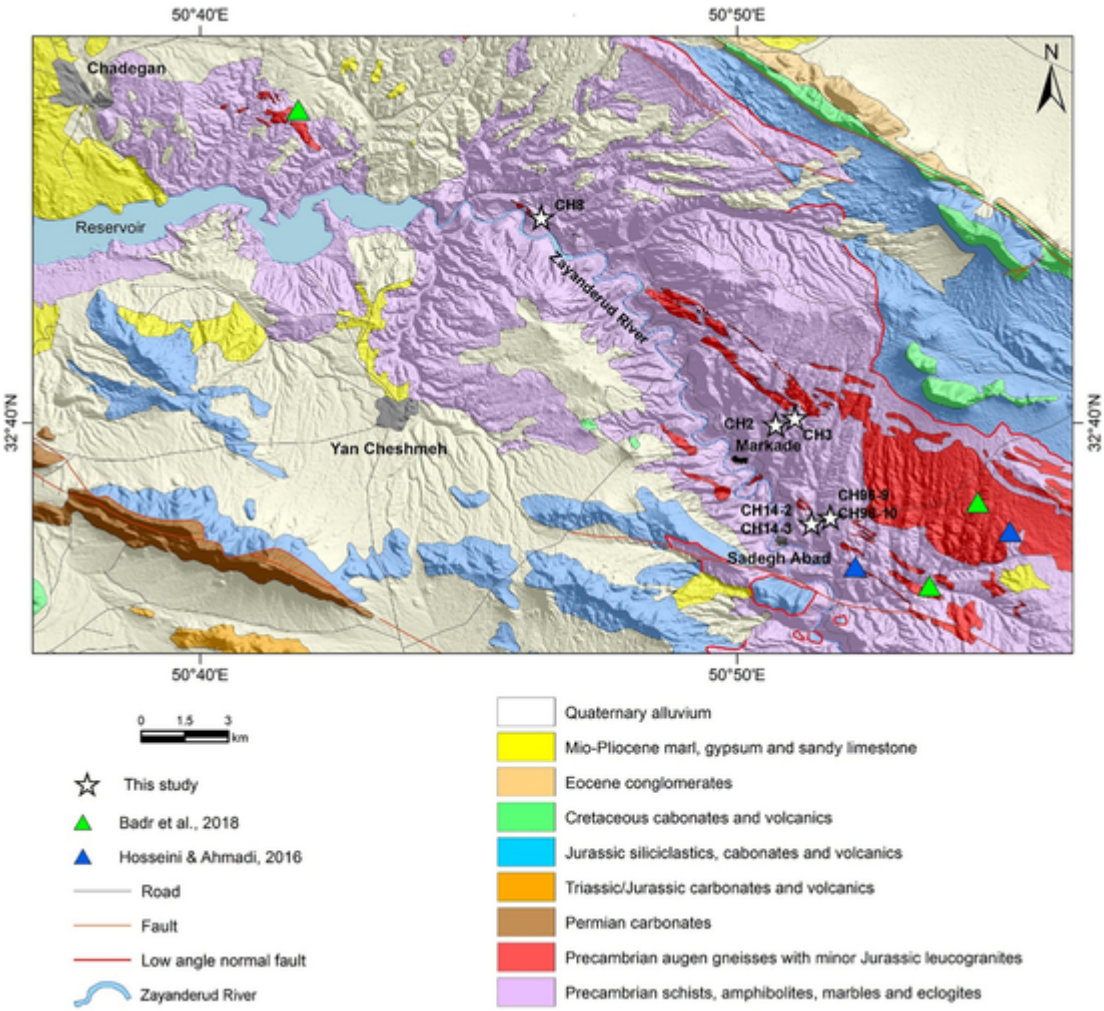

Fig. 2. Geologic map of the studied area on a shaded relief background (after Zahedi, 1993; Davoudian et al., 2016) showing locations of dated specimens. High pressure metamorphic rocks are best exposed along the upper Zayanderud River.

tween Chadegan and Sadeghabad (Fig. 2). The ZMC consists of mica schist, paragneisses, metagranite, metabasite, quartzite, and marble. The metabasites comprise eclogite, garnet amphibolite, and amphibolite. Chemically, the ZMC eclogites and metabasites are similar to continental back-arc (Malek-Mahmoudi et al., 2017) and continental flood basalts (Jamali Ashtiani, 2017). Amphibolites preserve evidence for a previous episode of HP metamorphism, such as rutile mantled by titanite, and symplectites of diopside and plagioclase (Fig. 3E) that are a retrogressive product of omphacite (e.g., Anderson and Moecher, 2007). Granitoid rocks of the ZMC are comparable in protolith age and lithology to other basement outcrops all along the SSZ, but a marked distinction is the presence of high-pressure metamorphic rocks including eclogite boudins (Davoudian et al., 2016). P-T estimates for eclogite and amphibolite-facies metamorphism are 21–24 kbar at 590–630 °C and 10–11 kbar at 650–700 °C, respectively (Davoudian et al., 2007). Structurally, the ZMC has the characteristics of a tectonic mélange occurring in a large-scale ductile shear zone (Davoudian et al., 2016) through which the deep NW-trending Zayanderud canyon has been incised (Fig. 2, Supplementary Fig. S1A).

Low-grade Precambrian strata that are age-equivalent to ZMC rocks are unconformably overlain by Permian carbonates and Jurassic volcano-sedimentary strata (Zahedi, 1976). A regional angular unconformity surface separates Cretaceous carbonates from older rocks in most places along the SSZ, but contacts between the Cretaceous limestone and the older rocks in the study area are generally fault-bounded (Fig. 2). Carbonate outcrops form elongate ridges of high topographic relief.

Eocene sediments are predominantly preserved along the northern border of the ZMC and consist of red beds dominated by polygenic conglomerates, which include abundant clasts of Cretaceous limestone, but lack metamorphic rock fragments. Poorly consolidated lacustrine deposits of light-colored marls and sandy limestones are attributed to the Miocene-Pliocene (Ghasemi et al., 1996); these sediments thinly drape the low-topography ZMC rocks over the entire region and are eroded by the incising Zayanderud River.

4. Samples and analyses

Four ZMC metagranites, two anatectic pegmatites, and their host mica schist have been selected for compositional and geochronological analyses. Locations and petrographic summaries of the studied samples are presented in Fig. 2 and Supplementary Table S1. For U—Pb zircon age determinations, three protomylonitic, one weakly- to non-porphyroclastic metagranite, and one sample from an anatectic pegmatite pocket were selected from different locations in the ZMC (Fig. 3). Zircon crystals from two dated samples were also analyzed for trace element compositions and O-isotopes to characterize the source and conditions of anatectic melting. Furthermore, three metagranites were analyzed for whole rock major and trace element compositions as a basis for comparison with results from previous studies (Hosseini and Ahmadi, 2016; Badr et al., 2018). White micas from mica schist and a crosscutting pegmatite were analyzed by electron microprobe and dated using the $^{40}Ar/^{39}Ar$ method.

Metagranites occur as variably sized bodies interspersed with mica schists and metabasites in the core of the ZMC (Fig. 1). Compositionally, they dis-

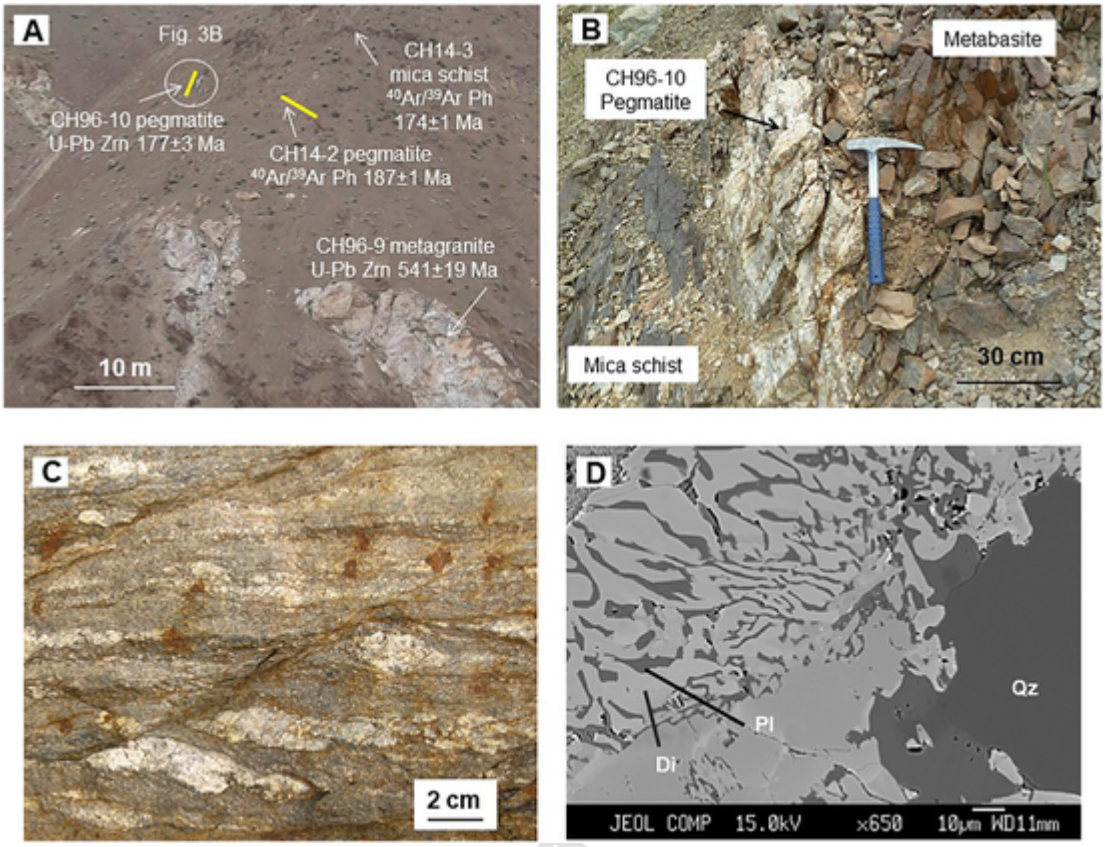

Fig. 3. A) Hillside view of metagranite intermingled with mica schists and sporadic metabasites, north of Sadeghabad. Four dated samples from this outcrop are marked. B) Anatectic pegmatite pod hosted by mica schist (left) and metabasite (right) at circle marked in A. C) Leucosomes aligned within the host mica schist ductile shear fabric on the left side of the pegmatite pod in B, suggesting syntectonic partial melting. D) Symplectite of diopside + plagioclase replacing primary omphacite in retrogressed amphibole eclogite (location shown in A and B).

play a range from granodiorites to granites. However, based on the abundance and size distribution of porphyroclasts, two end-members of mylonites are distinguished. The first type is a protomylonitic granitoid which is characterized by abundant K-feldpathic augen (Supplementary Fig. S1B-D). This rock type has yielded Ediacaran protolith ages (Nutman et al., 2014; Davoudian et al., 2016). Three of the measured samples (CH2, CH3 and CH8) belong to this type of metagranite. The second type shows distinctly more intense grain size reduction (Hosseini and Ahmadi, 2016; Badr et al., 2018) forming mylonite and ultramylonite (Supplementary Fig. S1C). These second-group mylonites mark zones of more intense strain compared to the protomylonitic granitoid locations and occur as parallel and up to decameters thick sheets and lenses within dark-colored host metamorphic rocks, creating a conspicuous zebra pattern around the Sadeghabad village on the northern side of Zayanderud River (Fig. 2 and Supplementary Fig. 1A). U—Pb zircon ages of Jurassic and Middle Cambrian have been attributed to this metagranite group (Hosseini and Ahmadi, 2016; Badr et al., 2018). Our measured sample CH96–9 represents this metagranite type.

Pegmatites and leucosomes have not been previously mentioned from the ZMC and were discovered in the course of our fieldwork. The outcrops described here are located ~1 km northeast of Sadeghabad (Fig. 2). In this location, mica schist dominates in outcrop, but it locally hosts isolated m- to dm-sized lenses of retrogressed amphibole eclogite along with an irregular network of patchy granitic leucosomes suggesting local melt segregation and accumulation (Fig. 3C,D). Leucosomes up to 3-cm long are common, but pegmatite pods are rare (Fig. 3). Thus far, we have mapped only two ~1 m- long pegmatite bodies in the Sadeghabad region (Fig. 3). The seeming scarcity of pegmatites at the outcrop scale is either due to their restricted occurrence, or them being mistaken for leuco-metagranite or quartz veins of similar appearance. The pegmatite sample CH96–10 is from a pocket that occurs along the contact between a darkly varnished m-sized boudined garnet-rich amphibole eclogite and a boudined sheet of leucogranite mylonites (Fig. 3A,B). It consists of light gray quartz and whitish sodic plagioclase, along with accessory apatite, titanite, garnet, biotite, epidote, and zircon. Pegmatite sample CH14–2 was collected in close proximity of sample CH96–10 (Fig. 2A), and contains cm-sized white-mica books of phengitic composition. The observed heterogeneity and large-crystal size preclude representative whole rock analyses of the pegmatites. Mica schist sample CH14–3 is also from the same outcrop as the pegmatite samples, and is a quartz-rich schist comprising plagioclase, white mica fish, garnet, biotite, rutile, zircon and opaque minerals. Some plagioclase crystals occur as large porphyroblasts. The white mica follows the foliation, wraps around the porphyroblasts, and parallels the fabric.

5. Analytical methods

5.1. Whole rock chemistry

Whole rock powders of three least altered protomylonitic to mylonitic granitoids were characterized by major and trace element analyses using the ICP-AES VARIAN Vista MPX instrument at Potsdam University, Germany. Data for major and trace element abundances are presented in Supplementary Table S2.

5.2. Microprobe analysis

White mica from pegmatite CH14–2 and its host mica schist CH14–3 were analyzed by electron microprobe using the five spectrometer JEOL JXA-8200 at University of Potsdam operating at 15 kV and 15 nA with a 2 μm beam diameter. Counting times were 10–20 s on peaks and half on background. Synthetic and natural standards were used. Data for white mica compositions are presented in Supplementary Table S3.

5.3. $^{40}Ar/^{39}Ar$ dating

White mica separates from pegmatite CH14–2 and its host mica schist CH14–3 were analyzed in the $^{40}Ar/^{39}Ar$ geochronology laboratory at the University of Potsdam. White mica in mica schist CH14–3 forms anastomosing foliation, grains are anhedral to subhedral, associated but not intergrown with chlorite. Some crystals are kinked and were avoided. White mica in pegmatite CH14–2 is a large, 2–3 cm long mica book and lacks deformation.

Routine procedures for $^{40}Ar/^{39}Ar$ geochronology follow Wilke et al. (2010) and Halama et al. (2014). A summary of analysis conditions for the samples in this study is presented in the Supplementary material. Age errors in the text and the figures are reported at two sigma (2σ) levels.

5.4. Ion microprobe zircon U—Pb, trace element and O-isotopes analyses

Mount preparation, imaging, as well as trace element and isotopic analyses using secondary ionization mass spectrometry (SIMS) were performed at the University of California, Los Angeles (UCLA) and Heidelberg University. Following zircon separation using conventional heavy liquid and magnetic techniques, the separated crystals were examined using a high-magnification binocular microscope. Rounded zircons were avoided, and only transparent, fracture-free and euhedral crystals were hand-picked. Crystals are doubly-terminated with generally long prismatic stems. The dimensions of the analyzed zircon crystals range from 40 to 200 and 100–450 μm in width and length, respectively, corresponding to aspect ratios between ~2 and 3. The selected grains were mounted in epoxy, polished and coated. Carbon coated mounts were used for cathodoluminescence (CL) imaging using a Tescan Vega-3 XMU variable-pressure SEM at UCLA, and a Zeiss-WITec RISE EVO MA15 with a Gatan ChromaCL2 detector at Heidelberg University. CL textures show narrowly spaced and often uninterrupted oscillatory zoning (Supplementary Fig. S2). Zircon crystals from the non-porphyroblastic granodiorite mylonite sample CH96–9 show broad zones and characteristically weaker CL emission than other samples. Some grains from pegmatite sample CH96–10 display truncated growth zones visible in CL (Fig. 4) which high spatial resolution SIMS geochronology identified as inherited cores. Further analytical details are provided in the Supplementary material. Age errors in the text and the figures are reported at two sigma (2σ) levels.

6. Results

6.1. Granitoid geochemistry

Silica and alkali oxide compositions of the studied rocks range from 70.4–71.4 wt% (SiO_2), 2.7–3.9 wt% (Na_2O), and 2.4–4.8 wt% K_2O (Supplementary Table S2). The samples plot in the granite field, near the granodiorite border in a total alkali vs. silica (TAS) diagram and show subalkaline affinity (Fig. 5A). Their magmatic arc character is pronounced as shown in the Rb vs (Y + Nb) discrimination diagram of Pearce et al. (1984) (Fig. 5B). There is some overlap of the data with the "Within plate granitoid" field in Fig. 5B as also emphasized by Badr et al. (2018), although the apparent A-type connection could merely be an artifact of extensive fractional crystallization of an I-type parental magma (Forster et al., 1997). The absence of minerals characteristic for anorogenic A-type granites such as alkaline Fe-rich pyroxenes and amphiboles (e.g., Li et al., 2012) also argues in favor of formation in a magmatic arc setting. There is also a conspicuous depletion of high-field strength elements (HFSE) relative to large ion lithophile elements (LILE) that is characteristic for arc granitoids (Fig. 5C).

6.2. Mineral chemistry

White micas in pegmatite and mica schist samples lack zoning and are mainly phengitic (Fig. 5D; Supplementary Table S3). Paragonite is rare and has only been found in some metagranites (Fig. 5D). In terms of Si-enrichment, white micas analyzed in the pegmatite and mica schist host are similar to phengites in ZMC eclogites near Chadegan (Fig. 5D), but their Ti contents are different (Fig. 5E). Auzanneau et al. (2010) have shown that Ti in phengite increases with temperature, whereas the relationship is inverted with pressure (Fig. 5E).

6.3. $^{40}Ar/^{39}Ar$ dating

Davoudian et al. (2016) have reported a range of phengite $^{40}Ar/^{39}Ar$ dates from 184 Ma to 173 Ma for a suite of eclogites from the ZMC. New $^{40}Ar/^{39}Ar$ dates on an anatectic pegmatite and the mica schist host (Supplementary Table S4) broadly agree with these published data. Large phengite crystals from the pegmatite sample CH14–2 yielded an average age of 186.9 ± 1.8 Ma (from steps 2 and 3 (Fig. 6A) which comprise 83% of the total $^{39}Ar_K$ released. The inverse isochron age from these two steps is 185.3 ± 2.4 Ma, and agrees with the average age, although the initial $^{40}Ar/^{36}Ar$ value exceeds the atmospheric value (295.5) outside 2 sigma error. Conservatively, the age of the white mica is thus reported as 185–187 Ma.

Mica schist sample CH14–3 yielded a plateau age of 174.3 ± 1.8 Ma, which meets the conditions of Fleck et al. (1977) by including more than three consecutive Ar release steps (Fig. 6B). The inverse isochron age for CH14–3 using the plateau steps is 169.5 ± 5.4 Ma with a poorly defined initial $^{40}Ar/^{36}Ar$ composition of 537 ± 123 (Fig. 6) overlapping the atmospheric value within 2 sigma error. The inverse isochron age of CH14–3 also agrees with the plateau age within 2 sigma uncertainty. An age of 170–174 Ma is assigned to CH14–3, although it remains unresolved if the apparent elevated initial $^{40}Ar/^{36}Ar$ results from excess ^{40}Ar, or from analytical uncertainty of ^{36}Ar which was close to the blank level. Regardless, these new dates agree with the 184–173 Ma $^{40}Ar/^{39}Ar$ age range previously reported for phengitic micas in the region (Davoudian et al., 2016).

6.4. U—Pb dating

A total of 121 spot analyses on selected zircon crystals from four different mylonitic granite samples was determined (Supplementary Table S5). Discordance, defined as the relative difference between the $^{206}Pb/^{238}U$ and $^{207}Pb/^{235}U$ ages normalized to the $^{206}Pb/^{238}U$ age, is within ±10% for most analyses, and is mostly due to the comparatively imprecise ^{207}Pb determination and its dependence on the common Pb correction. We therefore focus on $^{206}Pb/^{238}U$ ages which are concordant within uncertainty (Supplementary Fig. S3). Ignoring minor inheritance, analyses on the magmatic rims of zircon in the four analyzed mylonite samples show $^{206}Pb/^{238}U$ age ranges of 480–601 Ma (sample CH2), 412–601 Ma (sample CH3), 443–585 Ma (sample CH8) and 430–589 Ma (sample CH96–9). Extracting coherent age populations was performed using the "Zircon Age Extractor" algorithm (Ludwig, 2012), which accounts for the effects of inheritance and Pb-loss which often affects ancient high-pressure metamorphic rocks (e.g., Corfu, 2013). Ages of $551.8^{+4.2}/_{-20.9}$ (sample CH2), $567.3^{+14.7}/_{-10.3}$ (sample CH3), $564.7^{+9.1}/_{-5.2}$ (sample CH8) and $551.5^{+32.1}/_{-13.6}$ (sample CH96–9) Ma were obtained (Supplementary Fig. S4). We also applied the "Unmix Ages" algorithm in Isoplot 4.1 to model zircon age modes (Ludwig, 2012). For each sample, the number of components was incrementally increased, and their relative fractions were adjusted until the goodness of fit showed no further improvement. The resulting components for each sample correspond to the peak and shoulders shown in the $^{206}Pb/^{238}U$ age probability density plot (Fig. 7). The ages for the dominant mode were calculated at 551 ± 11 Ma, 571 ± 8 Ma, 566 ± 7 Ma and 541 ± 19 Ma. Younger zircon ages are interpreted as artifacts of Pb-loss and possibly overlap of the analysis spot onto younger (metamorphic) zircon domains. Because both statistical treatments result in closely overlapping ages for all samples, we pooled all available analyses, and obtained a coherent age average of 567.5 ± 5.5 Ma which comprises ~68% of the data points (Fig. 7E).

Spot analyses were also conducted on 10 sectioned zircon crystals from the anatectic pegmatite sample CH96–10 (Supplementary Table S5). Mostly, zircon rim domains were targeted, and interiors were only analyzed to confirm the presence of inherited cores, and the poten-

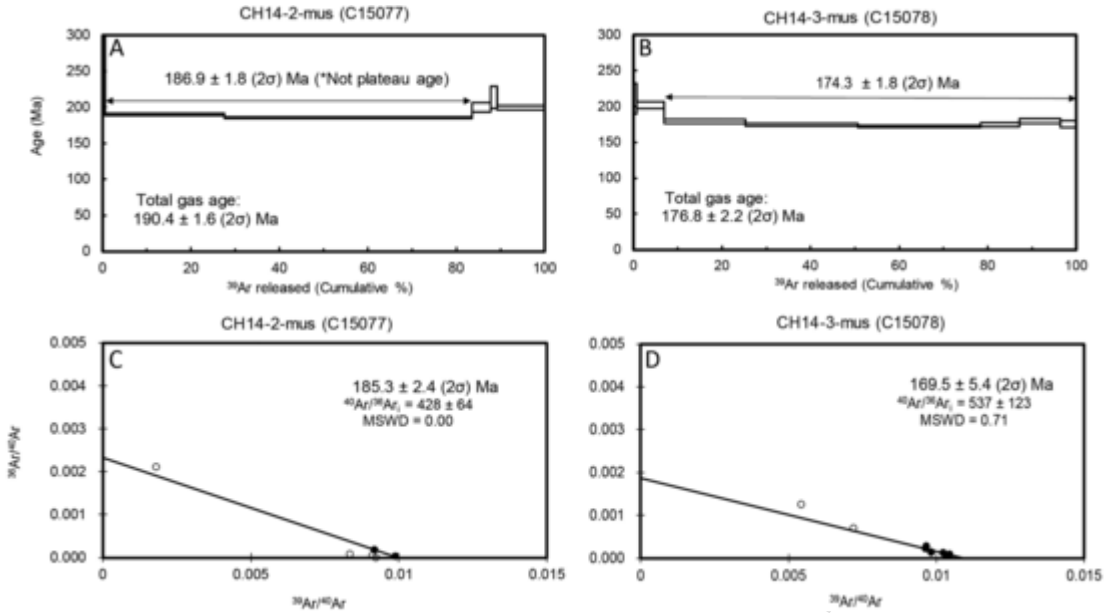

Fig. 6. $^{40}Ar/^{39}Ar$ age (Ma) spectra (A, C) and inverse isochron diagrams (B, D) for ZMC phengitic white micas. A-B) Pegmatite CH14–2. C-D) Mica schist CH14–3. In the age spectra, the total gas age and apparent average age (CH14–2) or plateau age (14–3) are given. Extent for average age or plateau is indicated by arrows. Inverse isotope correlation age is shown from the steps used for the average and plateau ages in the Ar release plots (black circles). Open circles are steps omitted from averaging.

and interior domains can produce mixed ages. Zircon rims in CH96–10 are characterized by very low Th/U values of <0.06, similar to zircon from pegmatites and leucosomes of the north Sulu ultrahigh-pressure terrane (Liu et al., 2010). Overall, rim $^{206}Pb/^{238}U$ zircon ages vary from 166 Ma to 243 Ma. The youngest data points (n = 18) yield a concordia age of 176.5 ± 3.2 Ma with an acceptable mean square of weighted deviates (MSWD) of concordance of 1.60 (Fig. 8). Older ages are interpreted as mixed ages from incomplete separation between rim and interior domains due to beam overlap. This was confirmed by placing multiple analysis spots onto a zoned zircon, which yielded a discordant $^{207}Pb/^{206}Pb$ age of 2724 ± 90 Ma for the core (CH96–10 27), whereas an analysis overlapping rim and core domains yielded a mixed $^{206}Pb/^{238}U$ age of 405 ± 38 Ma (CH96–10 21) without geological meaning (Figs. 4 and 8, Supplementary Table S5).

6.5. Zircon trace element abundances and thermometry

REE data for CH96–9 metagranite reveal steep positive slope patterns with positive Ce and negative Eu anomalies typical for magmatic zircons from silica-saturated igneous rocks (Fig. 9A) as represented by the coeval Hormuz Island Cadomian arc rhyolites (Faramarzi et al., 2015). Zircon crystals of CH96–10 pegmatite, however, are drastically different from typical igneous zircon and those in metagranite by showing low total REE (Supplementary Table S6), absence of significant negative Eu anomalies, and comparatively flat LREE (Fig. 9B). Ti-in-zircon thermometry was performed using the equation of Ferry and Watson (2007) for the presence of rutile and quartz (i.e. activities of TiO_2 and SiO_2 = 1.0). Temperatures of zircon crystallization for granodiorite mylonite CH96–9 show a range of 594–640 °C and a mean of 624 ± 21 °C (Fig. 10 and Supplementary Table S6). This is similar to the range of Ti-in-zircon thermometry results for zircon from granitic pegmatite CH96–10 is 600–744 °C with a mean of 638 ± 40 °C. These estimates are minimum temperatures because primary rutile is absent, although rutile is present as relics in nearby amphibole eclogite lenses, where it is often mantled by titanite. Ti-in-zircon temperatures for the granitic pegmatite are also at the upper limit of temperatures estimated for eclogite and the amphibolite-facies metamorphism (21–24 kbar at 590–630 °C and 10–11 kbar at 650–700 °C, respectively) as reported in the literature (Fig. 10).

6.6. Zircon $\delta^{18}O$ SIMS data

In situ O-isotope analyses were performed on the rims of 40 sectioned zircon crystals from metagranite sample CH96–9 and granitic pegmatite sample CH96–10 (Supplementary Table S7). Zircon crystals of the metagranite (CH96–9) reveal a homogeneous $\delta^{18}O$ composition of ca. +7‰ (Fig. 9C). These values are elevated compared to mantle zircon (+5.0‰ to +5.6‰; e.g., Valley, 2003), and are typical of continental arc magmas that are formed by mantle-derived magmas undergoing crustal assimilation or mixing with sediments and/or surficially altered volcanic rocks (Valley et al., 2005). Oxygen isotopic compositions for zircon rims of anatectic pegmatite sample CH96–10 show a wider $\delta^{18}O$ range (+1.19‰ to +8.49‰), yet the mean of 7.66‰ is very similar to that of the metagranite (Fig. 9D).

7. Discussion

7.1. Magmatic age of basement granitoids

The first geological map of the region attributed a Precambrian age to the metamorphic complex including its metagranites based on identifying a nonconformable contact between the Permian sediments and the metamorphic rocks (Zahedi, 1976). In a subsequent revision, a Jurassic age was proposed for the granitic protoliths based on an erroneous Jurassic age attributed to the protoliths of the metamorphic host rocks for these granites (Ghasemi et al., 1996). This age dispute has continued even after radiometric dating was introduced. Late Neoproterozoic (Ediacaran) U—Pb zircon ages of 586 ± 26 (Nutman et al., 2014), 569 ± 19 (Davoudian et al., 2016) and 560–586 Ma (Jamali Ashtiani et al., 2016) have been determined for the metagranites. Thus, despite five decades of field work, and several recent attempts for radiometric dating of the metagranites, no consensus has emerged on their granitic precursor ages and the timing of metamorphism. Our new zircon results indicate a magmatic crystallization age of 567.5 ± 5.5 Ma, which reinforces a link between ZMC metagranite protoliths and plutons from the Cadomian arc. For the highly mylonitized granite (sample CH96–9), our U—Pb zircon analyses produce a spread from 430 Ma to 589 Ma with a pronounced peak age at 541 ± 19 Ma, which we interpret as the timing of magmatic crystallization of the protolith (Fig. 7D). Younger, including the Middle Cambrian, ages are

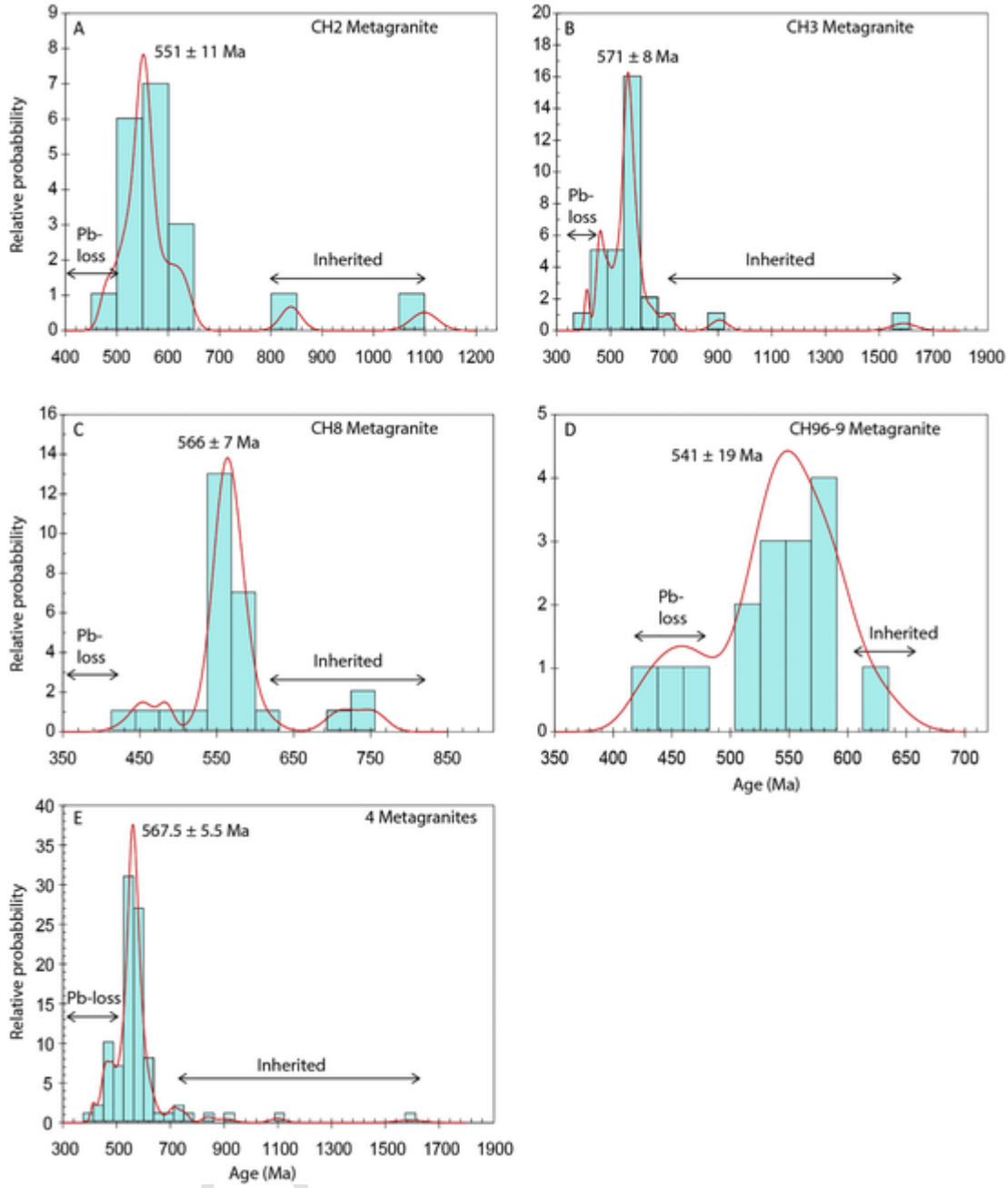

Fig. 7. Relative probability vs. $^{206}Pb/^{238}U$ age diagrams using Isoplot (Ludwig, 2012) for the ZMC metagranites. Dates older than the marked peaks are xenocrystic or possibly due to partial beam overlap onto xenocrystic domains, whereas younger dates most likely resulted from Pb-loss or partial beam overlap onto metamorphic rims.

the result of subsequent isotopic disturbances, as fluid-induced Pb-loss is well-known in high-pressure metamorphic rocks (e.g., Kröner et al., 2014).

7.2. Jurassic thermal overprint

Elsewhere in the Cadomian arc of southern Europe, the crystalline basement displays Alpine metamorphic-plutonic overprint. In the Menderes Massif of Western Turkey, which shows many similarities to the ZMC (Jamali Ashtiani, 2017), metamorphism and granite emplacement occurred in the Eocene and Miocene, respectively (Lips et al., 2001; Glodny and Hetzel, 2007). In the case of the ZMC, $^{40}Ar/^{39}Ar$ dates of 197 to 170 Ma determined for phengite from mica schists and eclogites indicate that the high-pressure metamorphism occurred already at least partly during the Early to Middle Jurassic (Davoudian et al., 2016; Jamali Ashtiani, 2017). Jurassic volcanism, manifested by andesitic volcanics in the ZMC cover strata, is well documented (Zahedi, 1976, 1993; Emami and Khalili, 2014), but the presence of age-correlated plutons in the ZMC has remained debated. Jurassic granitic bodies are certainly ubiquitous in the larger region (Fig. 1), but whether the 182 Ma leucogranites reported by Hosseini and Ahmadi (2016) are representing arc plutonism, or just local anatexis has thus far remained unresolved. In our field work, and after the long debate over the presence of Jurassic granites in the region, we discovered only minor volumes of leucosome and granitic pegmatite that resulted from partial melting of mica schists and retrogressed amphibole eclogites (Fig. 3). Nonetheless this discovery proves important in constraining the P-T-t trajectory of the ZMC (Fig. 10), and zircon rims crystallized in the pegmatite currently provide the best constraints for the age of peak metamorphism.

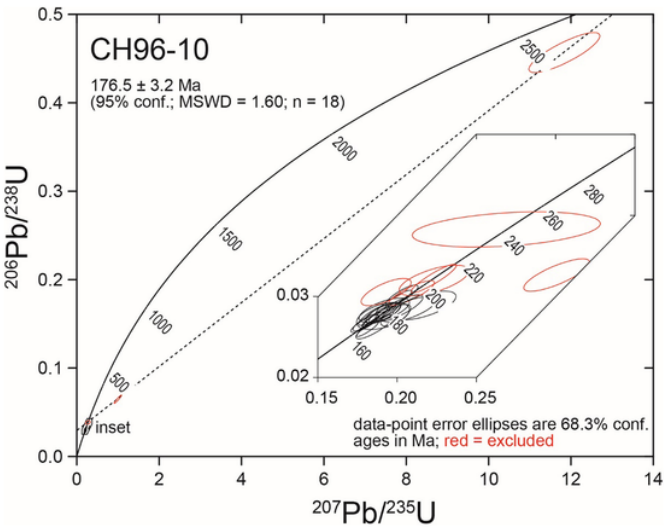

Fig. 8. Zircon U—Pb data for the anatectic pegmatite CH96–10. The youngest consistent population (n = 18) yields an age of 176.5 ± 3.2 Ma (2-sigma; MSWD = 1.60). Dashed line is a mixing line between the rim and interior of zoned zircon crystal (CH96–10 27).

The very low Th/U (Avg. 0.010, n = 25) in zircon from the pegmatite (CH96–10, Supplementary Table S6) is characteristic for pegmatites and granitic leucosomes in migmatites (Corfu, 2013). Also, the absence of negative Eu anomalies in zircon is in accord with melt generation from a source where plagioclase is absent or outweighed by other REE reservoirs (Rubatto, 2002). Moreover, these REE patterns are clearly distinct from those expected for subduction-related magmas, either of Cadomian or the Jurassic age. The overall low REE abundances along with a steeply increasing HREE pattern can be explained by incipient break-down of garnet in the mica schist and possibly the adjacent amphibole-bearing eclogite during retrogression as documented for the exhumation of other high-pressure terranes (Anderson and Moecher, 2007; Gilotti et al., 2014). In addition to residual garnet, REE may have also become sequestered in accessory apatite and/or titanite, which were stable and abundant during low-degree partial melting, resulting in low overall (L)REE abundance in pegmatite zircon.

Importantly, white mica in the pegmatite sample CH14–2 and the host mica schist sample CH14–3 is phengitic and compositionally very similar to the white mica analyzed from the eclogites in the region (Fig. 5D), which have defined the pressure peak in previous studies (Fig. 10). Quite remarkably, the U—Pb zircon age of the pegmatite is consistent with the $^{40}Ar/^{39}Ar$ age obtained for phengite in the same rock (Fig. 6). Therefore, we interpret the concordant $^{206}Pb/^{238}U$ zircon age of 176.5 ± 3.2 Ma (Fig. 8) supported by the overlapping $^{40}Ar/^{39}Ar$ dates for the oldest phengite in the eclogite suite (Davoudian et al., 2016) and the pegmatitic phengite (Fig. 6), as being close in time or only slightly postdating the pressure maximum reached by ZMC rocks. The older age of the large pegmatitic phengite (Fig. 6) is explained by grain-size dependence of closure temperature and its effect on Ar diffusion (Harrison et al., 2009; Scharf et al., 2016). Overall, these observations require a brief time interval between high-pressure metamorphism of continental crust, incipient exhumation, and partial melting during the Early Jurassic.

The timing of HP metamorphism in the ZMC along with rapid retrogression under HT conditions leading to anatexis is unique as it falls into the early stages of plate convergence and incipient subduction of the Neotethyan plate underneath Eurasia. We therefore advocate the hypothesis that the ZMC exemplifies an unexplored type of HP suite that has formed from continental protoliths (Davoudian et al., 2016; Malek-Mahmoudi et al., 2017; Jamali Ashtiani, 2017) in a subduction channel. This setting is a rather novel alternative for formation of HP rocks and deserves explanation.

Different scenarios for the timing and location of the Andean-type margin development along the Iran-side of the Neotethys exist. One hypothesis advocates that subduction started in the Cretaceous and was to the northeast of the SSZ (Lechmann et al., 2018; Azizi and Stern, 2019). However, others have advocated that oceanic subduction already began in the Late Triassic-Early Jurassic (ca. 200 Ma) (e.g., Berberian and King, 1981), and that the first active continental margin in it formed the core of the SSZ (Hassanzadeh and Wernicke, 2016; and references therein). Here, we follow this second scenario to provide a potential tectonic framework for high-P metamorphism in the ZMC rocks. Eclogite facies metamorphism of the Ediacaran continental basement rocks occurred at ≥184 Ma (Davoudian et al., 2016) (Fig. 10

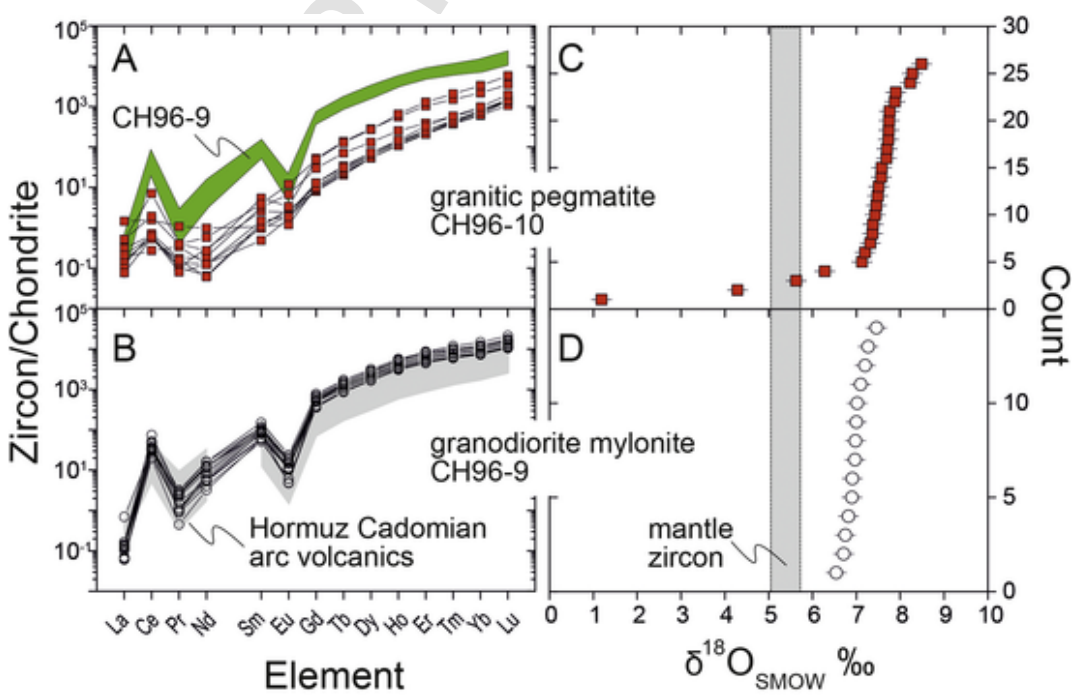

Fig. 9. Zircon geochemistry of two ZMC granitic rocks. A) Chondrite-normalized REE abundances of zircons from granitic pegmatite CH96–10 and B) Leucogranodiorite mylonite CH96–9. The Hormuz Island Cadomian arc volcanics (Faramarzi et al., 2015) are added for comparison. Chondrite data are from McDonough and Sun (1995). C) Values of $\delta^{18}O$ for zircons from anatectic pegmatite CH96–10 and D) leuco-metagranite CH96–9. Mantle zircon data are from Valley (2003).

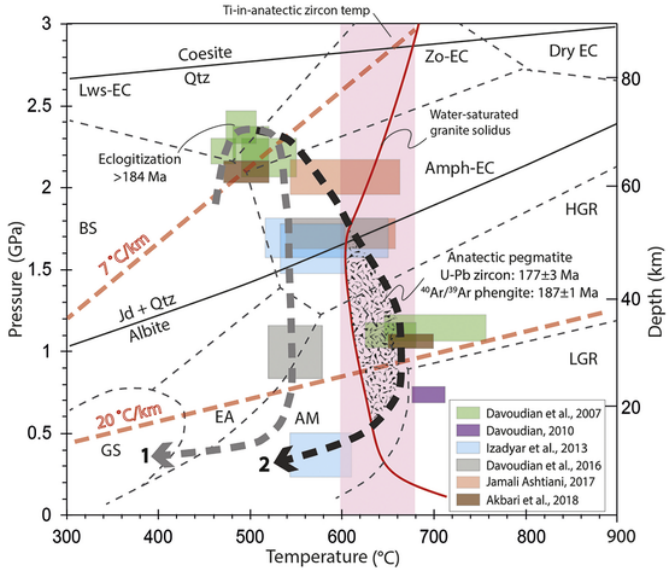

Fig. 10. Simplified P-T diagram, compiling mineral thermobarometry data from the literature with new thermometry constraints from ZMC pegmatite. The pressure peak (timing unknown) is defined by garnet-omphacite-phengite-rutile assemblage, whereas the temperature peak is constrained by the Ti-in-zircon thermometer and the corresponding U—Pb zircon age. Paths 1 and 2 are discussed in the text. Red curve indicates the wet solidus from Stern and Wyllie (1981). P-T-t paths 1 and 2 are discussed in the text. AM, amphibolite facies; Amp-EC, amphibole eclogite facies; BS, blueschist facies; Dry-EC, dry eclogite facies; EA, epidote amphibolites facies; GS, greenschist facies; HGR, high-pressure granulite facies; LGR, low-pressure granulite facies; Lws-EC, lawsonite eclogite facies; Zo-EC zoisite eclogite facies. Eclogite $^{40}Ar/^{39}Ar$ phengite dates are from Davoudian et al. (2016). (For interpretation of the references to colour in this figure legend, the reader is referred to the web version of this article.)

), and partial melting of the associated mica schist was at 177 ± 6 Ma (Fig. 10). The deep subduction of continental rocks of the ZMC and their partial exhumation (Fig. 11) thus occurred ca. 150 million years before the mid-Tertiary Arabia-Eurasia collision in the Zagros orogen (Pirouz et al., 2017). In this case, continental collision may not represent the only mechanism for generating HP rocks from continental protoliths (Fig. 11A).

The ultimate exhumation history of the ZMC high-grade rocks is not the focus of the current contribution (cf. Verdel et al., 2007; Malekpour-Alamdari et al., 2017), but the absence of metamorphic clasts in Eocene sediments suggests burial until then. For the early part of the exhumation trajectory, we propose buoyant escape (Thomson et al., 1999) as the driving force for uplift due to the overall low density of dominantly felsic rocks intensified by incipient melting in the high-P rocks (Fig. 11). Partial melting of the high-grade rocks in the ZMC, hence, deserves further investigation.

7.3. Anatexis and its implications for timing of peak pressure and subduction initiation

Constraining conditions and timing of metamorphism in the ZMC is critical for unraveling the events associated with subduction initiation along the northeastern passive margin of the Neotethys Ocean. Existing mineral thermobarometry data have been compiled and are plotted on a P-T diagram (Fig. 10). The pressure peak is defined by eclogites from the vicinity of Chadegan village at the northwestern end of the ZMC (Davoudian et al., 2016). A major uncertainty about the pressure peak is its timing, which remains yet to be determined. Two distinct exhumation paths have been suggested based on existing data (Fig. 10). Path 1 indicates isothermal exhumation (Davoudian et al., 2016), and path 2 is a clockwise retrograde trajectory following peak pressure metamorphism defined by most of the retrogressed mineral assemblages (Fig. 10). Although path 1 may apply to the best-preserved eclogite boudins sporadically exposed near the western end of the complex (Davoudian et al., 2016), our data suggest that, upon exhumation from the subduction channel, most of the ZMC became heated to temperatures equivalent to the wet biotite-granite solidus of ≥610 °C (Stern and Wyllie, 1981) (path 2, Fig. 10). Indications of incipient melting are extensive in the region and deserve more field and laboratory investigation in the future. Some evidence for partial melting as pre-

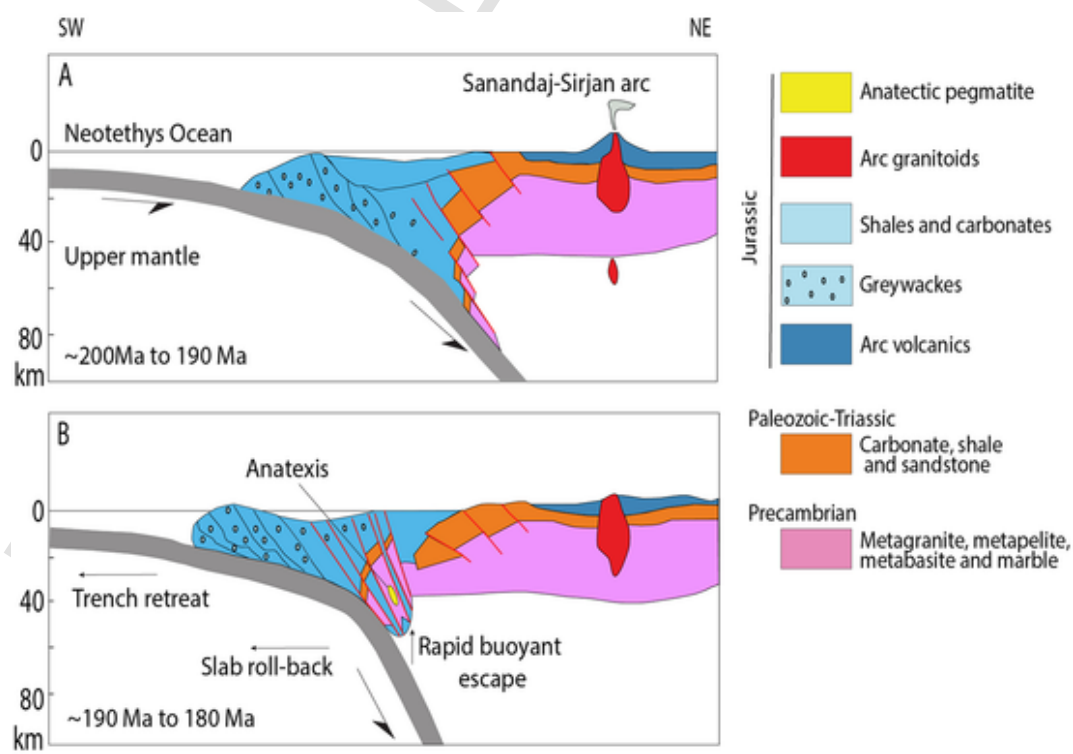

Fig. 11. Geodynamic significance of the CH96–10 and CH14–2 anatectic pegmatites. A) Foundering of continental crust to depths of ca. 80 km where eclogite-grade metamorphism occurred. Retrograde anatexis occurred following subduction initiation at the northeastern margin of the Neotethys Ocean in the Early Jurassic. B) Partial melting associated with rapid exhumation driven by buoyant escape and probable decoupling resulted from slab-rollback.

sented here includes ubiquitous quartzofeldspathic leucosomes in the mica schists (e.g., sample CH14–3; Fig. 3D) associated with relatively rare anatectic pegmatites (samples CH14–2 and CH96–10; Fig. 3C). White micas in both rock types are phengitic and comparable with white micas in eclogite in terms of Si and alkali contents (Fig. 5A); phengite from the mica schist and pegmatite, however, is more enriched in Ti, suggesting crystallization under higher temperatures and/or lower pressures (Fig. 5E). Ti-in-zircon thermometry for pegmatite sample CH96–10 yields a minimum crystallization temperature of 638 ± 40 °C (Supplementary Table S6; Fig. 10), which overlaps with the retrograde portion of the proposed P-T path 2, supporting field evidence that the ZMC assemblage intercepted the wet granite solidus upon decompression. The U—Pb zircon age of 176.5 ± 3.2 Ma obtained for the same pegmatite is overlapping with $^{40}Ar/^{39}Ar$ dates of white micas (Section 6.3), which provides a robust constraint for the retrograde P-T trajectory (Fig. 10). Based on this new age for the thermal peak, the timing for the pressure maximum experienced by ZMC rocks can be estimated based on precedence for rapid exhumation of eclogite-facies HP in a modern setting: in eastern Papua New Guinea, eclogite formed at depth of ca. 75 km depth before ca. 4.3 Ma is now exposed on the Earth's surface, suggesting exhumation at plate tectonic rates (Baldwin et al., 2004). Numerical simulation has also shown that exhumation at plate velocity rates is feasible (Gerya et al., 2002). Assuming an exhumation rate of 1 cm/a for the ZMC rocks, they must have been exhumed from ~70 km depth in only 3 Ma to ~40 km depth where partial melting took place (Fig. 10). This suggests a timing of 183 ± 6 Ma for the pressure peak. By adding the time required for burial of the Eurasian passive margin to a depth of ca. 70 km at an equivalent rate, this timing would be consistent with subduction initiation at ca. 200 Ma (Arvin et al., 2007; Hassanzadeh and Wernicke, 2016).

8. Conclusions

U—Pb zircon geochronology resolves persistent controversies regarding the protolith age of the voluminous metagranite association in central Iran and sheds light on a previously undetected Early Jurassic partial melting event in the ZMC basement-related metamorphic-plutonic complex of the Zagros hinterland north of Shahrekord. The dominant zircon population yields an age of 567.5 ± 5.5 Ma for all protomylonitic and mylonitic granitoids. This confirms the presence of Ediacaran granitic intrusions as in other blocks of crystalline continental basement of Iran. Minor recent Pb-loss or partial beam overlap onto narrow metamorphic zircon rims likely caused a displacement to younger ages, but no reliable Jurassic zircon crystallization ages were found for these bodies. These ages, however, were detected in a granitic pegmatite which formed by partial melting of largely amphibolite grade mica schists and associated metabasite lenses during retrogression. Pegmatite U—Pb zircon ages are concordant at 176.5 ± 3.2 Ma, and corresponding Ti-in-zircon minimum temperatures average 638 ± 40 °C. Oxygen isotopes of pegmatite zircons, and the presence of inherited zircon cores, is consistent with partial melting of mica schist with possibly minor contribution from metabasite upon decompression. This age marks the timing of the temperature peak of metamorphism and the beginning of anatexis. The surrounding mica schist yielded $^{40}Ar/^{39}Ar$ phengite ages that overlap with the $^{206}Pb/^{238}U$ zircon age of the pegmatite. This reveals rapid cooling immediately after high-pressure metamorphism of a deeply subducted continental assemblage. The ZMC thus represents a unique example of pre-collisional burial of a passive margin along the Alpine-Himalayan orogenic belt during the onset of subduction in the Neotethys Ocean at about 200 Ma. These results encourage utilizing geodynamic modelling to investigate the possibility of deep sinking of an old rifted margin at the onset of subduction.

Supplementary data to this article can be found online at https://doi.org/10.1016/j.gr.2020.01.005.

Declaration of competing interest

The authors declare that they have no known competing financial interests or personal relationships that could have appeared to influence the work reported in this paper.

Uncited references

Davoudian, 2010
Davoudian et al., 2006
Izadyar et al., 2013

Acknowledgments

This article is based largely on the lead author's dissertation at the Shahid Beheshti University (SBU), Tehran, Iran. Comments on an earlier version by Janet Harvey improved the English. The quality of the presentation was greatly improved by constructive reviews from Bob Stern, Jean-Pierre Burg and two anonymous reviewers, and editorial guidance from Taras Gerya. Discussions with Brian Wernicke on involvement of passive margin in subduction initiation have been helpful. Support from the SBU, Institute of Earth and Environmental Science of Universität Potsdam, and DAAD is acknowledged. The ion microprobe facility at UCLA is partly supported by a grant from the Instrumentation and Facilities Program, Division of Earth Sciences, National Science Foundation. DFG support for the Heidelberg Ion Microprobe facility is acknowledged. Mortaza Pirouz is thanked for helping with the ArcGIS compilations of map figures.

References

Akbari, K, Tabatabaei Manesha, S M, Parfenova, O V, 2018. Petrology and rare Earth elements Mineral Chemistry of Chadegan Metabasites (Sanandaj-Sirjan Zone, Iran): evidence for Eclogite-Facies Metamorphism during Neotethyan Subduction. Geochem. Int. 56 (7), 670–687.

Anderson, E D, Moecher, D P, 2007. Omphacite breakdown reactions and relation to eclogite exhumation rates. Contrib. Mineral. Petrol. 154, 253–277. doi:10.1007/s00410-007-0192-x.

Arvin, M, Pan, Y, Dargahi, S, Malekizadeh, A, Babaei, A, 2007. Petrochemistry of the Siah Kuh granitoid stock southwest of Kerman, Iran: implications for initiation of Neotethys subduction. J. Asian Earth Sci. 30, 474–489.

Auzanneau, E, Schmidt, M W, Vielzeuf, D, Connolly, J A D, 2010. Titanium in phengite: a geobarometer for high temperature eclogites. Contrib. Mineral. Petrol. 159, 1–24. doi:10.1007/s00410-009-0412-7.

Azizi, H, Stern, R J, 2019. Jurassic igneous rocks of the central Sanandaj–Sirjan zone (Iran) mark a propagating continental rift, not a magmatic arc. Terra Nova 31, 415–423. doi:10.1111/ter.12404.

Badr, A, Davoudian, A, Shabanian, N, Azizi, H, Asahara, Y, Neubauer, F, Dong, Y, Yamamot, K, 2018. A- and I-type metagranites from the North Shahrekord metamorphic complex. Iran: Evidence for Early Paleozoic post-collisional magmatism, Lithos 300–301, 86–104.

Baldwin, S L, Monteleone, B D, Webb, L E, Fitzgerald, P G, Grove, M, Hill, E J, 2004. Pliocene eclogite exhumation at plate tectonic rates in eastern Papua New Guinea. Nature 431, 263–267.

Berberian, M, King, G C P, 1981. Towards a paleogeography and tectonic evolution of Iran. Can. J. Earth Sci. 18, 210–265.

Condie, K C, 2014. Growth of continental crust: a balance between preservation and recycling. Mineral. Mag. 78 (3), 623–637.

Corfu, F, 2013. A century of U-Pb geochronology: the long quest towards concordance. Geol. Soc. Am. Bull. 125, 33–47.

Davoudian, A, 2010. Mineral chemistry and P-T crystallization conditions of the Zayanderud granitoids, North Shahrekord. Iranian Journal of Crystallography and Mineralogy 18 (3), 497–512.

Davoudian, A R, Khalili, M, Noorbehesht, I, Dachs, E, Genser, J, Shabanian, N, 2006. Geochemistry of metabasites in the north of the Shahrekord. Sanandaj-Sirjan Zone, Iran, Neues Jahrbuch fur Mineralogie- Abhandlungen 182, 291–298.

Davoudian, A R, Genser, J, Dachs, E, Shabanian, N, 2007. Petrology of eclogites from north of Shahrekord, Sanandaj- Sirjan Zone. Iran, Mineralogy and Petrology 92, 393–413.

Davoudian, A, Genser, J, Neubauer, F, Shabanian, N, 2016. $^{40}Ar/^{39}Ar$ mineral ages of eclogites from North Shahrekord in the Sanandaj-Sirjan Zone, Iran: Implications for the tectonic evolution of Zagros orogeny. Gondwana Res. 37, 216–240.

Emami, S N, Khalili, M, 2014. Volcanic and subvolcanic rocks dating in the north of Shahrekord by $^{40}Ar/^{39}Ar$ method, a new approach regarding the occurrence and duration of the Jurassic volcanism in the Sanandaj-Sirjan zone. Petrology 5 (18), 1–15.

Faramarzi, N S, Amini, S, Schmitt, A K, Hassanzadeh, J, Borg, G, McKeegan, K, Razavi, S M H, Mortazavi, S M, 2015. Geochronology and geochemistry of rhyolites from Hormuz Island, southern Iran: a new record of Cadomian arc magmatism in the Hormuz Formation. Lithos 236–237, 203–211.

Ferry, J M, Watson, E B, 2007. New thermodynamic models and revised calibrations for the Ti-in-zircon and Zr-in-rutile thermometers. Contrib. Mineral. Petrol. 154 (4), 429–437.

Fleck, R J, Sutter, J F, Elliot, D H, 1977. Interpretation of discordant $^{40}Ar/^{39}Ar$ age-spectra of Mesozoic tholeiites from Antarctica. Geochim. Cosmochim. Acta 41, 15–32.

Forster, H J, Tischendorf, G, Trumbull, R B, 1997. An evaluation of the Rb vs. (Y+Nb) discrimination diagram to infer tectonic setting of silicic igneous rocks. Lithos 40, 261–293.

Gerya, T V, Stöckhert, B, Perchuk, A L, 2002. Exhumation of high-pressure metamorphic rocks in a subduction channel: a numerical simulation. Tectonics 21 (6), 1056. doi:10.1029/2002TC001406.

Ghasemi, A, Hajhosseini, A, Hosseini, M, 1996. Geological Map of Iran Sheet

Glodny, J, Hetzel, R, 2007. Precise U–Pb ages of syn-extensional Miocene intrusions in the central Menderes Massif, western Turkey. Geol. Mag. 144, 235–246. doi:10.1017/S0016756806003025.

Halama, R, Konrad-Schmolke, M, Sudo, M, Marschall, H, Wiedenbeck, M, 2014. Effects of fluid-rock interaction on $^{40}Ar/^{39}Ar$ geochronology in high-pressure rocks (Sesia-Lanzo Zone, Western Alps). Geochim. Cosmochim. Acta 126, 475–494.

Harrison, T M, Célérier, J, Aikman, A B, Hermann, J, Heizler, M T, 2009. Diffusion of ^{40}Ar in muscovite. Geochim. Cosmochim. Acta 73, 1039–1051.

Hassanzadeh, J, Wernicke, B P, 2016. The Neotethyan Sanandaj-Sirjan zone of Iran as anarchetype for passive margin-arc transitions. Tectonics 35, 586–621.

Hassanzadeh, J., Stockli, D., F., Horton, B. K., Axen, G. J., Stockli, L.D., Grove, M., Schmit, A. K., Walker, J.D., 2008. U- Pb zircon geochronology of late Neoproterozoic-Early Cambrian granitoids in Iran: implications for paleogeography, magmatism, and exhumation history of Iranian basement, Tectonophysics 451, 1–4, 71–96.

Hosseini, B, Ahmadi, A R, 2016. Geochemistry and U-Pb Dating of North Saman Granitoid Rocks, Geoscience Quarterly Journal 100, 109–120. Geological Survey of Iran, Tehran.

Hunziker, D, Burg, J P, Pierre Bouilhol, P, von Quadt, A, 2015. Jurassic rifting at the Eurasian Tethys margin: Geochemical and geochronological constraints from granitoids of North Makran. southeastern Iran, Tectonics 34, 571–593. doi:10.1002/2014TC003768.

Izadyar, J, Mousavizadeh, M, Eram, M, 2013. Metamorphic evolution of high-pressure Quartz Schists in the Chadegan metamorphic complex, Sanandaj-Sirjan zone, Iran. Journal Geope 3 (2), 1–20.

Jamali Ashtiani, R, 2017. High Grade Metamorphic Rocks from North of Shahrekord, Sanandaj-Sirjan Zone: Age, Fabric, Geneses. Shahid Beheshti University, Tehran, Iran, Dissertation (195 p).

Jamali Ashtiani, R, Hassanzadeh, J, Schmitt, A K, Rahgoshay, M, Sobel, E, 2016. Final assembly of Gondwana along its northern margin: revising the suture geometry based on evidence from the Iranian-Turkish Plateau. EGU Abstract # 2399.

Kröner, A, Wan, Y, Liu, X, Liu, D, 2014. Dating of zircon from high-grade rocks: which is the most reliable method? Geosci. Front. 5, 515–523.

Lechmann, A, Burg, J P, Ulmer, P, Mohammadi, A, Guillong, M, Faridi, M, 2018. From Jurassic rifting to Cretaceous subduction in NW Iranian Azerbaijan: geochronological and geochemical signals from granitoids. Contrib. Mineral. Petrol. 173 (12), 102. doi:10.1007/s00410-018-1532-8.

Li et al., 2012. Geochronology, geochemistry, and Nd–Hf isotopes of early Palaeozoic–early Mesozoic I-type granites from the Hufang composite pluton, Fujian, South China: crust–mantle interactions and tectonic implications. International Geology Review, 54, 15–32. doi:https://doi.org/10.1080/00206814.2010.496542

Lips, A L W, Cassard, D, Sozbilir, H, Yilmaz, H, Wijbrans, J R, 2001. Multistage exhumation of the Menderes Massif, western Anatolia (Turkey). Int. J. Earth Sci. 89, 781–792.

Liu, F, Robinson, P T, Gerdes, A, Xue, H, Liu, P, Liou, J G, 2010. Zircon U–Pb ages. REE concentrations and Hf isotope compositions of granitic leucosome and pegmatite from the north Sulu UHP terrane in China: Constraints on the timing and nature of partial melting, Lithos 117 (1–4), 247–267.

Ludwig, K R, 2012. Isoplot/Ex Version 4: a Geochronological Toolkit for Microsoft Excel. Berkeley Geochronology Center, special publication 5, 1–75.

Malek-Mahmoudi, F, Davoudian, A, Shabanian, N, Azizi, H, Asahara, Y, Neubauer, F, Dong, Y, 2017. Geochemistry of metabasites from the North Shahrekord metamorphic complex, Sanandaj-Sirjan Zone: Geodynamic implications for the Pan-African basement in Iran. Precambrian Res. 293, 56–72.

Malekpour-Alamdari, A, Axen, G, Heizler, M, Hassanzadeh, J, 2017. Large-magnitude continental extension in the northeastern Iranian Plateau: Insight from K-feldspar 40Ar/39Ar thermochronology from the Shotor Kuh–Biarjmand metamorphic core complex. Geosphere 13 (4). doi:10.1130/GES01423.1.

McDonough, W F, Sun, S S, 1995. The composition of the Earth. Chem. Geol. 120, 223–253.

Moghadam, H S, Li, X H, Stern, R J, Santos, J F, Ghorbani, G, 2016. Age and nature of 560-520 calc-alkaline granitoids of Biarjmand, northeast Iran: insights into Cadomian arc magmatism in northern Gondwana. Int. Geol. Rev. 1492–1509.

Nutman, A P, Mohajjel, M, Bennett, V C, Fergusson, C L, 2014. Gondwanan Eoarchean–Neoproterozoic ancient crustal material in Iran and Turkey: zircon U–Pb–Hf isotopic evidence. Can. J. Earth Sci. 51, 272–285. doi:10.1139/cjes-2013-0138.

Pearce, J A, Harris, N B W, Tindle, A G, 1984. Trace element discrimination diagrams for the tectonic interpretation of granitic rocks. J. Petrol. 25, 956–983.

Pirouz, M, Avouac, J-P, Hassanzadeh, J, Kirschvink, J L, Bahroudi, A, 2017. Early Neogene foreland of the Zagros, implications for the initial closure of the Neo-Tethys and kinematics of crustal shortening. Earth Planet. Sci. Lett. 477, 168–182.

Ramezani, J, Tucker, R D, 2003. The Saghand region, central Iran: U-Pb geochronology, petrogenesis and implications for Gondwana tectonics. Am. J. Sci. 303, 622–665.

Rubatto, D, 2002. Zircon trace element geochemistry: partitioning with garnet and the link between U–Pb ages and metamorphism. Chem. Geol. l84, 123–138.

Scharf, A, Handy, M R, Schmid, S M, Favaro, S, Sudo, M, Schuster, R, Hammerschmidt, K, 2016. Grain-size effects on the closure temperature of white mica in a crustal-scale extensional shear zone — Implications of in-situ $^{40}Ar/^{39}Ar$ laser-ablation of white mica for dating shearing and cooling (Tauern Window, Eastern Alps). Tectonophysics 674, 210–226.

Stern, R, 1994. Arc assembly and continental collision in the Neoproterozoic East African orogen: implications the consolidation of Gondwanaland. Annu. Rev. Earth Planet. Sci. 22, 319–351.

Stern, C R, Wyllie, P J, 1981. Phase relationships of I-type granite with H20 to 35 Kilobars: the Dinkey Lakes biotite-granite from the Sierra Nevada Batholith. J. Geophys. Res. 86 (B11), 10412–10422.

Thomson, S.N., Stcökhert, B., and Brix, M.A., 1999. Miocene high-pressure metamorphic rocks of Crete, Greece: Rapid exhumation by buoyant escape, in Ring, U., et al., eds., Exhumation processes: Normal faulting, ductile flow and erosion: Geological Society [London] Special Publication 154, p. 87–108.

Valley, J W, 2003. Oxygen isotopes in zircon. In: Hanchar, J M, Hoskin, P W O (Eds.), Zircon, Reviews in Mineralogy and Geochemistry, 53. Mineralogical Society of America/Geochemical Society, Washington, DC, pp. 343–385.

Verdel, C, Wernicke, B P, Ramezani, J, Hassanzadeh, J, Renne, P R, Spell, T L, 2007. Geology and thermochronology of Tertiary Cordilleran-style metamorphic core complexes in the Saghand region of central Iran. Geol. Soc. Am. Bull. 119 (7/8), 961–977.

Wilke, F D H, O'Brien, P J, Gerdes, A, Timmerman, M J, Sudo, M, Khan, M A, 2010. The multistage exhumation history of the Kaghan Valley UHP series, NW Himalaya, Pakistan from U-Pb and $^{40}Ar/^{39}Ar$ ages. Eur. J. Mineral. 22, 703–719.

Yang, T N, Chen, J L, Liang, M J, Xin, D, Aghazadeh, M, Hou, Z Q, Zhang, H R, 2018. Two plutonic complexes of the Sanandaj-Sirjan magmatic-metamorphic belt record Jurassic to Early Cretaceous subduction of an old Neotethys beneath the Iran microplate. Gondwana Res. 62, 246–268.

Zahedi, M, 1976. Explanatory Text of the Esfahan Quadrangle Map, 1:250,000. Geological Survey of Iran, F8, p. 49.

Zahedi, M. 1993, Shahrekord quadrangle map, 1:250,000, Geological Survey of Iran, E8.